Published in final edited form as:
J Mol Biol. 2013 March 11; 425(5): 944–957. doi:10.1016/j.jmb.2012.12.016.

Vibriocholerae cytolysin recognizes the heptasaccharide core of complex N-glycans with nanomolar affinity

Sophia Levan[a], **Swastik De**[a], and **Rich Olson**[a,*]

[a]Department of Molecular Biology and Biochemistry, Wesleyan University, 52 Lawn Avenue, Middletown, Connecticut, USA

Abstract

Pathogens selectively target host cells using adhesion molecules and secreted virulence factors that may utilize protein, lipid, or carbohydrate ligands on the cell surface. The human intestinal pathogen *Vibrio cholerae* secretes a pore-forming toxin, *Vibrio cholerae* cytolysin (VCC), which contains two domains that are structurally similar to known carbohydrate-binding proteins. These tandem domains are attached to the carboxy-terminus of the cytolytic domain and contain a β-trefoil fold and a β-prism fold. VCC has been shown to bind glycosylated proteins, and removal of the β-prism domain leads to a large decrease in lytic activity against rabbit erythrocytes. Despite these clues, the identity of the glycan receptors of VCC and the role of glycan binding in toxin activity remains unknown. To better understand this specificity, we used a combination of structural and functional approaches to characterize the carbohydrate-binding activity of the VCC toxin. We first probed the monosaccharide-binding activity of VCC and demonstrated that the toxin exhibits millimolar affinity for aldohexoses. To understand this specificity, we solved the crystal structure of the VCC β-prism domain bound to methyl-α-mannose. Next, we utilized a mammalian glycan screen to determine that the β-prism domain preferentially binds complex N-glycans with a heptasaccharide $GlcNAc_4$ Man_3 core (NGA2). Fluorescence anisotropy and surface plasmon resonance indicated an approximately 100-nanomolar affinity of the β-prism domain for the heptasaccharide core. Our results suggest that carbohydrate-binding domains on the VCC toxin facilitate high-affinity targeting of mammalian cell membranes, which may contribute to the ability of VCC to lyse cells at picomolar concentrations.

Keywords

pore-forming toxin; cholera; lectin; complex N-glycan; hemolysin

Introduction

Cholera is a diarrheal disease caused by colonization of the human intestine by the aquatic bacterium *Vibrio cholerae.* In 2010, roughly 300,000 cases were described worldwide

[*]**Corresponding Author**: Rich Olson, Ph.D., Assistant Professor, Department of Molecular Biology and Biochemistry, Wesleyan University, 224 Hall-Atwater, 52 Lawn Ave., Middletown CT, 06459-0175, USA, Phone: 860-685-3070, Fax: 860-685-2141, rolson@wesleyan.edu.

Accession Numbers:
Coordinates and structure factors have been deposited in the Protein Data Bank with accession number 4GX7.

resulting in 7,500 deaths.[1] Following consumption of contaminated water, *V. cholerae* passes through the stomach and attaches to the mucosal epithelium of the small intestine. Due to the acid sensitivity of the organism, bacteria that survive the stomach must divide rapidly in order to establish a viable colony. Eventually, a quorum sensing system activates classical cholera toxin (CT) secretion resulting in the massive efflux of fluid and viable bacteria out of the gut and into the environment.[2]

As a defensive measure against innate immune cells, *V. cholerae* secretes toxins and virulence factors to support colonization. Two of these secreted agents, the multifunctional, autoprocessing repeat in toxin (MARTX) protein and *Vibrio cholerae* cytolysin (VCC, or hemolysin), are essential for low-dose colonization in mouse models[3,4] and are markers of the O1 El Tor *V. cholerae* strain, which is largely responsible for the seventh global cholera pandemic. VCC is a β-pore-forming toxin (PFT) that lyses rabbit erythrocytes, human neutrophils, and human intestinal cells in culture[5–7] by inserting a 14-stranded β-barrel channel into the membrane. Expression of VCC occurs preferentially during early stages of infection[8] via regulation by the HapR quorum sensing mechanism.[9] At this time, the subset of cells targeted by VCC in the human body is not well established; however, it was recently shown that neutrophils are important in preventing *V. cholerae* from invading extra intestinal organs.[10] This indicates that innate immune cells would make an attractive target for lysis by VCC.

The mechanism by which β-PFTs like VCC cause cellular damage and lysis has been made clearer by structural studies outlining the transition between secreted water-soluble and assembled membrane-imbedded states. VCC is structurally homologous to *Staphylococcus aureus* α-hemolysin[11] and γ-leukocidin.[12] All three β-PFTs form large channels in cell membranes with inner diameters ranging from approximately 8–18 Å at their narrowest constrictions.[13] The established paradigm for the assembly of β-PFTs begins with the secretion of a water-soluble monomer, which binds to the membrane through specific lipid, protein, and/or carbohydrate interactions. Binding to the membrane reduces a three-dimensional search to a two-dimensional search[14]; thereby facilitating oligomerization into a non-lytic pre-pore state.[15] Conformational rearrangements lead to coordinated insertion of the amphipathic loops and formation of the lytic channel.

How toxins initially recognize membranes varies from protein to protein, and understanding the basis for this selectivity is important if therapeutic measures are to be successful in reducing intoxication by secreted bacterial factors. The utilization of specific carbohydrate receptors by bacterial toxins is a common strategy, with prime examples including cholera toxin subunit B binding to the GM_1 ganglioside[16], *Aeromonas hydrophila* aerolysin binding to N-linked sugars on glycosyl phosphatidyl inositol-anchored proteins[17], and *Streptococcus mitis* lectinolysin binding to Lewis y and b glycans.[18] In many cases, distinct carbohydrate-binding domains with lectin-like folds mediate the interaction with glycan targets.

The crystal structure of the VCC water-soluble monomer[19] revealed two carboxy-terminal domains with lectin-like folds (Figure 1A). The first domain consists of a β-trefoil fold also found in the plant toxin ricin[20] and the human mannose receptor.[21] The second lectin-like domain has a β-prism fold common in many plant lectins, such as *A. integrifolia* artocarpin[22], jacalin[23], *G. sp* griffithsin[24], and the *M. pomifera* agglutinin.[25] Additionally, this fold is found in the insect larvae-targeting *B. thuringiensis* δ-endotoxins[26], which also form toxic channels in membranes.

Carbohydrate-binding activity for VCC has been demonstrated previously, with β_1-linked galactosyl glycans suggested as receptors for the toxin.[27] Treatment of erythrocytes with neuraminidase increases the hemolytic activity of the toxin, suggesting that sialylation of

glycans reduces the ability of VCC to bind to the membrane. Co-crystallization[19] of the VCC monomer with β-octyl glucoside (β-OG) revealed a binding site within the VCC β-prism domain and hydrogen-bonding interactions between the side chain of Asn[617] and hydroxyl groups on the C4 and C6 positions of the glucose moiety (Figure 1B). Variants of VCC missing the terminal β-prism domain[5] exhibit significantly decreased lytic activity (as much as 1000-fold) against rabbit erythrocytes[19,28] even though these mutants still form ring-like structures reminiscent of the full-length protein.[28,29] These results suggest that the VCC β-prismdomain may play a functional role in the membrane-targeting activity of the toxin even if the specific identity of these receptors is not well understood.

To probe the specificity of VCC for putative membrane receptors, we characterized the carbohydrate-binding specificity and affinity of VCC using a combination of structural and functional techniques. We first measured VCC binding to mono- and disaccharides by isothermal titration calorimetry (ITC) and solved the structure of the β-prism domain bound to methyl-α-mannose, an aldohexose derivative. We next conducted a screen against a panel of 611 mammalian glycans and showed that VCC binds to complex N-glycans, but not oligomannose or hybrid N-glycans. We demonstrate that the isolated β-prism domain binds the heptasaccharide complex N-glycan core (NGA2) with an affinity of approximately 100 nM. The glycan screen indicates that modification of the NGA2 core with Lewis X type sugars, such as those found on human neutrophils, improves binding and that sialylation is detrimental to VCC binding. In competition assays, NGA2 reduces the hemolytic activity of the toxin suggesting that sugar-derived compounds could be useful as anti-toxin therapeutics. Together, these results define the affinity of VCC for physiologically relevant glycans and suggest possible cellular targets of the toxin.

Results

The VCC β-prism Domain Contributes to Cytolytic Activity

The X-ray crystal structure of the VCC monomer (Figure 1A) revealed two structural domains with folds similar to β-trefoil and β-prism carbohydrate-binding lectins.[19] VCC lyses rabbit red blood cells (rRBCs) at picomolar concentrations, with a lytic activity approximately 6-fold higher than human erythrocytes.[27] As demonstrated previously[28], a variant of VCC missing the carboxy-terminal β-prism domain (VCC_{Trunc}) displays roughly 1000-fold decrease in hemolytic activity against rRBCs (Figure 2). The dramatic loss in activity of the VCC_{Trunc} variant against rRBCs could be due to the loss of a high-affinity carbohydrate-binding site or disruption of the mechanism of assembly and pore formation due to the loss of the β-prism domain.

In an effort to diminish or disrupt the carbohydrate-binding activity of VCC without removing the β-prism domain, we individually mutated Asn[617] to alanine to remove putative hydrogen-bonding partners and lysine to sterically block the pocket. Each of these mutations caused a roughly 50-fold loss in activity over wild type illustrating that disruption of the carbohydrate-binding site leads to a loss of hemolytic activity. The fact that the loss in activity of these mutants is not as severe as complete removal of the β-prism domain leaves open the possibility that the truncated toxin is less able to form pores. However, functional channels still form at higher total protein concentration as evidenced by the similarly-shaped hemolysis curve and electron cryo-microscopy structures of truncated toxin pores.[29,30] Further determination of the specificity of VCC for cell-surface glycans is necessary to understand the specific cellular receptors of the VCC β-prism domain and the role these sugars play in cell lysis.

Determination of Mono- and Disaccharide Specificity

Lectin proteins often display specificity towards monosaccharides, oligosaccharides, or a combination of both. Because the VCC crystal structure identified VCC binding to a single detergent molecule with a glucoside headgroup, we decided to start outlining the specificity of the β-prism domain using common monosaccharide sugars found at the termini of cell-surface glycans. To determine the selectivity and affinity of the β-prism domain for simple sugars, we conducted a series of binding experiments using isothermal titration calorimetry (ITC). To improve protein solubility and expression yield, we cloned and expressed the β-prism domain as a separate poly-histidine tagged construct ($VCC_{\beta\text{-prism}}$). In all cases, binding isotherms indicated one-to-one binding of mono- and di-saccharides to $VCC_{\beta\text{-prism}}$ or full-length VCC (VCC_{WT}).

To begin, we measured the affinity of $VCC_{\beta\text{-prism}}$ for three aldohexoses: D-glucose, D-galactose, and D-mannose (Table 1 and Figure S1) that differ in the stereochemistry of hydroxyl residues on the 5-carbon ring. Interestingly, $VCC_{\beta\text{-prism}}$ bound one molecule each of glucose and mannose with low millimolar affinity (K_D values of 12.0 mM and 14.8 mM, respectively), but did not exhibit any measurable galactose-binding activity. This suggests that $VCC_{\beta\text{-prism}}$ prefers an equatorial hydroxyl at the C4 position (D-galactose is axial at C4) and does not recognize the difference in hydroxyl stereochemistry at C2 between glucose and mannose. $VCC_{\beta\text{-prism}}$ did not exhibit measurable binding to L-fucose, which is missing a C6 hydroxyl and exhibits L rather than D stereochemistry, nor N-acetyl-D-glucosamine, a glucose derivative with a bulky N-acetyl moiety on C2 (Figure S2).

Monosaccharide-binding lectins may possess anomeric specificity and demonstrate a higher affinity for C1 substituents in the α or β position. To determine whether $VCC_{\beta\text{-prism}}$ exhibits anomeric specificity, we measured binding to five monosaccharides with methoxy groups on C1 in α or β conformations. $VCC_{\beta\text{-prism}}$ bound Me-α-D-mannose and Me-α-D-glucose slightly better than D-mannose and D-glucose (K_D values of 3.2 and 7.1 mM, respectively), but did not bind Me-α-D-galactose, Me-β-D-glucose, or Me-β-D-galactose. This suggests that the β-prism domain is specific for α-glycosides of mannose and glucose.

To extend our investigation to longer carbohydrate chains, we evaluated $VCC_{\beta\text{-prism}}$ binding to two disaccharides (Table 1 and Figure S2): maltose (glucose-α1,4-glucose) and cellobiose (glucose-β1,4-glucose). $VCC_{\beta\text{-prism}}$ bound maltose but did not bind cellobiose, confirming that the β-prism domain prefers α-glycosides. The K_D for the binding of maltose (30.9 mM) was 10-fold less than the K_D for Me-α-mannose binding (Table 1), indicating that the glucose-α1,4-glucose motif is a poor β-prism ligand. The increased affinity for methylated sugars suggests that the natural substrate of the β-prism domain may be an oligosaccharide that contains an α-glycoside moiety.

To assess whether the monosaccharide-binding activity measured for the $VCC_{\beta\text{-prism}}$ domain reflects the binding activity of full-length VCC_{WT}, ITC was used to measure the binding affinity of VCC_{WT} for Me-α-D-mannose (Table 1 and Figure S3). The K_D of binding to VCC_{WT} (1.5 mM) was similar to the K_D of binding to $VCC_{\beta\text{-prism}}$ (3.2 mM) confirming that the binding specificity and affinity of the isolated β-prism domain is representative of the carbohydrate-binding specificity of the holotoxin. We also measured binding of Me-α-D-mannose to the D617K mutant of VCC and could not detect measurable binding. This indicates that the D617K mutant negates binding to monosaccharide sugars (within our detection limits), although it is still possible that more complex oligosaccharides retain some binding affinity.

Crystal Structure of $VCC_{\beta\text{-prism}}$ Bound to Me-α-Mannose

To gain a better picture of the interactions that determine monosaccharide specificity, we crystallized and solved the structure of $VCC_{\beta\text{-prism}}$ bound to the tightest-binding substrate from our ITC studies: Me-α-D-mannose. The $VCC_{\beta\text{-prism}}$ crystals contained 6 copies per asymmetric unit (Figure 3A) and diffracted to approximately 2.85 Å (Figure S4). All six monomers contained clear density for a single Me-α-D-glucose molecule (Figure 3B) in a similar position to the β-octyl glucoside molecule seen in our previous crystal structure.[19]

Lectin-carbohydrate interactions are generally stabilized by hydrogen-bonding and hydrophobic interactions. The main-chain and side-chain interactions between the protein and sugar are consistent with the data obtained from the ITC experiments and explain the preference for α-glucosides. Three possible hydrogen bonds between the β-prism domain and Me-α-D-mannose were identified using the Chimera FindHBond function using the constraints outlined in Mills et al.[31,32] One additional hydrogen bond satisfies the geometric criteria when H-bond constraints are relaxed by 0.4 Å and 20°. These bonds were between the carboxyl group of Asp^{617} and the hydroxyl on C4 of Me-α-D-mannose (explaining the specificity of glucose and mannose over galactose), the backbone amide nitrogen of Gly^{632} and the hydroxyl on C3 of Me-α-D-mannose, and between the backbone amide nitrogen of Ala^{614} and O1 of Me-α-D-mannose (Figure 3B). An additional putative hydrogen bond that satisfied relaxed constraints was identified between the backbone amide nitrogen of Ala^{615} and the hydroxyl C6 of Me-α-D-mannose (indicating why L-fucose does not bind). The hydroxyl on C2 points away from the binding pocket and does not form hydrogen bonds with the protein. This clarifies why the β-prism domain exhibits similar binding to glucose and mannose, but does not necessarily rule out binding of N-acetyl glucosamine. The lack of binding observed for this sugar may result from steric constraints induced by the bulky substitution or interactions between the N-acetyl group and the C1 hydroxyl that influence the anomeric conformation.

The O-linked C1 methyl group of Me-α-mannose faces the sidechain of Tyr^{654} making a non-polar interaction consistent with the roughly five-fold increase in affinity of Me-α-D-mannose over D-mannose. Substitution of a β-linkage at this position may disrupt this interaction or create a steric clash leading to the loss of binding to Me-β-D-mannose observed in the ITC experiments. Interestingly, VCC does bind to β-octyl glucoside (detergent micelle effects made it impossible for us to measure the affinity by ITC) although the extended alkyl tail makes additional hydrophobic interactions that might overcome the non-ideal stereochemistry of the C1 substituent.

While the structural insights are consistent with the binding data, the millimolar affinity of VCC for simple sugars is unsatisfying in light of the picomolar activity of VCC against rRBCs and the 1000-fold loss of activity for the VCC^{Trunc} protein. Clearly, the cellular targets recognized by VCC are more complex than terminal residues on cell-surface glycans.

Glycan Chip Screening

To broaden our search for glycan targets of VCC, we labeled VCC_{WT} and VCC_{Trunc} with a fluorescent dye (Alexa Fluor 488) and conducted a screen against 611 mammalian glycan structures in collaboration with the Consortium for Functional Glycomics. Printed glycan microarrays consist of a combinatorial library of glycan molecules chemically attached to a glass slide. Proteins specific for a unique glycan motif will bind to few sugars on the microarray, while lectins with broad specificity will bind to a larger subset of targets.[33] Results are obtained in relative fluorescence units (RFUs) and do not provide absolute affinity values, but do provide relative affinities of the target protein for different glycans.

Labeled VCC_{WT} at a concentration of 10 μg/mL bound to a number of related glycans within the dynamic range of the screen (Figure 4). The average RFU for the entire screen was 361 with nine glycans scoring above 5,000 RFUs and four above 10,000 RFUs. The top four strongest binders consisted of an asialo-, agalacto-biantennary heptasaccharide (NGA2) core, NGA2 decorated with two β-1,3-linked galabiose (galactose-α-1,4-galactose) groups, NGA2 decorated with two β-1,3-linked galactose groups (forming a terminal lacto-N-biose group), and NGA2 with two Lewis X groups (galactose-β-1,4(fucose-α-1,3)N-acetyl glucosamine) in order from lowest to highest RFUs. Intriguingly, all but two (#352 and #347) of the top twenty-five glycans identified in the screen (Figure S5) contained identical bi-antennary NGA2 cores commonly found in complex N-glycans (sugar #4 in Figure 4).

To determine which of the two VCC lectin-like domains was responsible for the binding profile obtained for VCC_{WT}, we also screened VCC_{Trunc} protein against the 611-glycan screen. No significant binding was observed with the VCC_{Trunc} protein, indicating that the β-prism domain is responsible for the observed glycan-binding activity. This suggests that the β-trefoil domain does not exhibit high-affinity glycan binding to any of the sugars present in the screen and further supports our hypothesis that the addition of the β-prism domain at some point in the evolutionary history of VCC led to a loss of carbohydrate-binding activity within the β-trefoil domain.[19] This point is also supported by the observation that the β-prism domain is not found in *V. vulnificus* and *A. hydrophila* hemolysins.

The utility of the glycan screen resides not only in the carbohydrate ligands identified by the screen, but also in the carbohydrates not bound by the protein. The terminal Lewis X, galabiose, and lacto-N-biose fragments enhanced binding when attached to the complex glycan core; however, none of these isolated fragments yielded greater than 100 RFUs by themselves (Figure S6). VCC weakly binds smaller fragments of the NGA2 core, with the core pentasaccharide ($GlcNAc_2Man_3$, #51) only garnering 1,153 RFUs. Additionally, the screen rules out binding to high-mannose and hybrid type N-glycans, as well as many cores with more than two antennae.

A closer look at the highest-affinity glycans allows us to make several observations regarding the stereochemical preferences for β-prism domain binding. The addition of an α-1,6 fucose to the N-acetylglucosamine adjacent to the asparagine in the core is a common modification found in vertebrates.[34] Modification of the second strongest binder (#325 with 19,702 RFUs) with a core fucose decreased binding significantly (#355 with 5,670 RFUs), and modification of a related sugar (#54 with 5,026 RFUs) had a similar effect (#354 with 1,732 RFUs). Core fucosylation of the highest-affinity binder (#328 with 21,665 RFUs) reduced the signal to negligible levels (#420 with 238 RFUs). The addition of N-acetylneuraminic acid (a sialic acid) to the termini of the highest-affinity glycans in the screen generally decreased observed VCC binding as shown by comparing #54 (5,026 RFUs) with the α-1,6 sialated #57 (1,846 RFUs) or the α-1,3 sialated #327 (2,106 RFUs). While a number of cap structures are tolerated, the most common forms with sialic acid linked to the galactose generally gave poor signals (Figure S5). The effects of the decoration of glycans with sialic acid and its implications for the possible action of neuraminidase will be further elaborated on in the Discussion. Although we see some variation in binding activity depending on the type of substrate the glycan is attached to (compare #53 NGA2 attached to glycine with 11,490 RFUs to #52 attached to asparagine with 4,237 RFUs), the general trends regarding core fucosylation and sialylation hold.

The results from the glycan screen suggest that VCC primarily recognizes the NGA2 heptasaccharide core. The binding site will tolerate modification of the terminal N-acetyl glucosamine with β-1,3 and β-1,4 galactose moieties, with three particular modifications

leading to a measured increase in RFUs. These additional groups may fine-tune interactions between the glycan and the protein, although it remains to be seen whether these shifts in relative binding have physiological implications with regard to the activity of VCC against cells. VCC may target a limited subset of glycans with high-affinity (like the Lewis X derivative or a glycan not represented in the screen), or it may be sufficient to broadly recognize a wide array of complex N-glycans with varying affinity. Levels of modifications like sialylation and core fucosylation could further render cells more or less sensitive to the toxin.

Determination of Complex N-Glycan Affinity

The glycan screen identified carbohydrates recognized by VCC, but did not offer a quantitative measure of affinity in molar terms. To understand how well VCC binds N-glycans, we measured the affinity of VCC for the NGA2 complex N-glycan core (#4 in Figure 4) using two independent biophysical methods. First, we measured the binding of $VCC_{\beta\text{-prism}}$ to a 2-aminobenzoic acid (2-AA)-labeled NGA2 sugar by monitoring the change in fluorescence anisotropy of the dye upon binding (Figure 5A). From these data we obtained a single site K_D of 71 ± 65 nM, roughly five orders of magnitude stronger than the monosaccharide-binding affinity to hexose sugars. Binding to the $VCC_{\beta\text{-prism}}$ D617A mutant was decreased to a K_D of 20 μM ± 6.1 μM (Figure S7). This indicates that the glycan-binding activity is attenuated but not eliminated, clarifying why the VCC_{WT} D617A mutant showed a level of hemolytic activity greater than the VCC_{Trunc} mutant (Figure 2). We next measured binding of $VCC_{\beta\text{-prism}}$ to unlabeled NGA2 by surface plasmon resonance (Figure 5B). Fitting to a single-site kinetic model provided a result consistent with the anisotropy data, with a K_D of 108 nM and association and dissociation rates of 37,000 $M^{-1}s^{-1}$ and 0.040 s^{-1}, respectively. Extrapolating these data to the glycan screening data, we might expect binding to the highest affinity binders identified in the screen (#1–3 in Figure 4) to be even tighter than to the NGA2 core alone.

Competition of VCC Hemolytic Activity

If binding to cell-surface glycans is important for the high-affinity lytic activity of VCC, competition by NGA2 should lead to a decrease in the hemolytic activity of the toxin. To address this possibility, we conducted hemolysis assays with increasing amounts of NGA2 to look for an effect of the glycan on lysis. We saw a dose-dependent delay in the half-life of lysis at NGA2 concentrations up to 10 μM, or roughly 100-fold the measured K_D (Figure 6A). This indicates that NGA2 can slow the lytic activity of VCC against rRBCs (Figure 6B), presumably by competing with cell-surface glycans. Competition with Me-α-mannose within the same concentration range had no effect (Figure 6B). Due to the difficulty in obtaining higher concentrations in NGA2, we were not able to saturate the effect. This may arise from the observed fast off-rate of the NGA2 core, which allows the toxin to eventually find the optimal glycan receptor on the cell surface, or from the high valency of the interaction of the VCC heptamer with multiple glycans on the cell surface. Furthermore, binding to these surface glycans may bring the toxin close to additional determinants of membrane binding (such as lipids or protein receptors) that makes binding to the membrane surface virtually irreversible within the time frame of the experiment.

Discussion

ITC and glycan array screening revealed that the β-prism domain of VCC exhibits specificity for biantennary complex N-glycans with nanomolar affinity. This is the only example, to our knowledge, of specificity for complex N-glycans in both a β-prism lectin fold and in a bacterial pore-forming toxin. N-glycans are covalently attached to glycoproteins at an asparagine residue by an N-glycosidic bond and are expressed in all

Eukaryra; however, protists, fungi, plants, and invertebrates lack the carbohydrate-processing machinery required to synthesize complex N-glycans.[34] This fact, along with the requirement for cholesterol in target membranes[35], supports the notion that VCC targets mammalian cell membranes. This is in contrast with other *V. cholerae* effectors that have antimicrobial[36] or anti-amoeba[37] activities, as is observed with proteins associated with the type VI secretion pathway of *V. cholerae*. Selective binding of surface glycans would lead to increased monomer density at the cell membrane enhancing the ability of VCC to bind and assemble into transmembrane channels. When glycan binding is interrupted by removing or mutating the β-prism domain, we observe a significant decrease in the activity of the toxin against rRBCs.

Specificity for N-glycans has been observed in lectins from a variety of taxa. PP2-A1 phloem lectin from Arabidopsis and KSA-2 lectin from *Kappaphycus striatum* are specific for high mannose N-glycans.[38,39] Similarly, the *Oryza sativa* lectin expressed in rice[40], the fungal mitotic lectin from *Rhizoctonia bataticola*[41], and the GNA-related lectin from maize[42] are all specific for complex N-glycans. Additionally, a structure of a C-type lectin from the sea bivalve *Codakiaorbicularis* was determined to 1.3 Å bound an Asn-linked nonasaccharide.[43] While these lectins provide other examples of N-glycan targeting proteins, they all exhibit folds distinct from the VCC β-prism domain.

The results of the glycan screen provide additional insights into the breadth of potential cellular targets of VCC. The glycan with the largest binding signal is terminated with a Lewis X motif (Galβ1-4(Fucα1-3)GlcNAc(β1-2)). This marker is also known as CD15, is found on the surface of neutrophils[44], and is upregulated in certain cancers.[45,46] Lewis X sugars are targeted by other pathogenic virulence factors, including the SabA adhesion molecule of *H. pylori*[47], toxin A from *C. difficile*[48], and the SSL5 super-antigen from *S. aureus*[49]; however, none of these proteins are structurally homologous with VCC.

CD15 ligands are important in the selectin-mediated rolling of leukocytes along the vascular epithelium, but are also found in the colon and intestinal epithelium.[50,51] Neutrophils are highly susceptible to attack by VCC[7] and have been proposed as a possible target of VCC.[52] Neutrophils are also the primary cell type responsible for confining *V. cholerae* to the intestine, and strains missing accessory toxins (VCC and MARTX toxin) are rapidly cleared from the gut.[10] Furthermore, VCC expression is negatively correlated with quorum[9] and could serve as a defensive mechanism during the early stages of intestinal colonization. Neutrophil-expressed CD15 would make an enticing Achilles heel for a cytolytic toxin to attack, but further study will be required to determine how significant these ligands are in determining VCC cellular tropism.

Additional NGA2-modifying groups identified by the glycan screen include Galβ1-3 and Galβ1-4 terminal sugars. The Galβ1-4 GlcNAc motif is referred to as a Type 2 glycan unit and is found on most cell types.[34] In contrast, the Galβ1-3 GlcNAc motif is referred to as a Type 1 glycan unit. This motif is found exclusively on the epithelia of human gastrointestinal and reproductive tracts, is upregulated in many cancers when found on O-glycans[53], and is a target of cholera heat-labile enterotoxin.[54] Preferential binding to Type 1 glycan units suggests that the β-prism domain of VCC may also have an affinity for human gastrointestinal epithelia, although the absolute strength of this interaction and local concentration of toxin will determine whether the VCC toxin damages the epithelium during infection.

Outlining the site where complex N-glycans bind to the VCC β-prism domain will require further structural work. The heptasaccharide NGA2 core contains three mannose residues, all of which contain sugars attached to the C1 position. Our ITC data and crystal structure of

$VCC_{\beta\text{-prism}}$ bound to Me-α-mannose suggest that bulky groups attached to the C1 position reduce the ability of ligands to bind to the domain. This loss in affinity might be rescued by additional interactions between the heptasaccharide and protein, or the entire glycan may utilize a different mode of binding to the β-prism domain. We observe that a nearby residue, Trp^{706}, adopts different rotamer positions across the six $VCC_{\beta\text{-prism}}$ molecules in the crystal structure asymmetric unit (Figure S8). In five molecules, the residue is flush with the protein surface (closed) and in a sixth the residue swings outward to make crystal contacts with a neighboring polypeptide chain (open). The outward position opens a cleft that could accommodate part of an extended glycan chain. In the VCC heptamer structure (PDB 3O44) all fourteen copies of the β-prism are in the closed position and in the VCC monomer structure bound to β-OG (PDB 1XEZ), the residue is in the open position. The flexible nature of this side-chain may allow interactions with portions of bound glycans in the open state, a hypothesis which further structural studies will address.

The identification of N-glycan cores as a VCC target helps to explain several observations made previously regarding interactions between VCC and glycosylated proteins and the preference for rabbit over human red blood cells. VCC activity is inhibited by glycosylated proteins such as fetuin[27], with a significant increase in inhibition upon desialylation of the glycoprotein. Structural analysis of glycans on fetuin indicate a heterogeneous mixture of bi- and tri-antennary complex N-linked glycans including peripheral β1,3 and β1,4-linked galactose residues.[55–57] Our glycan screen identified sugar cores found on fetuin and showed a preference for the desialylated versions of these ligands. *V. cholerae* secretes a neuraminidase containing a central enzymatic domain flanked by two lectin domains. Glycan-chip screening indicate that the neuraminidase lectin domains exhibit specificity for sialylated versions of β1,4-linked galactose moieties attached to complex N-glycan cores.[58] These results support a model where secreted neuraminidase removes terminal sialic acid residues from complex N-glycans thereby generating new receptors for VCC. This may serve to confine VCC activity to the intestinal epithelium or to enhance specificity for glycans recognized by both neuraminidase and VCC.

The pronounced increased activity of VCC against rabbit erythrocytes over human and sheep erythrocytes[27,59] may derive from the glycan repertoire expressed on the cell surface. It has been observed that mouse sperm cells bind very tightly to rabbit erythrocytes, but not to human, mouse, rat, goat, sheep, cow, horse, dog, or cat erythrocytes.[60] Analysis of rabbit erythrocyte glycans by mass spectrometry indicates an abundance of bi-antennary complex N-glycans terminated with repeating Gal-β1,4-GlcNAc moieties[61], which might enhance the lytic activity of VCC towards these cells. Staphylococcal α-hemolysin also shows a preference for rabbit erythrocytes over human; however, this partiality is mediated by binding of the metalloprotease ADAM-10.[62] While VCC may also utilize a yet-unidentified protein receptor, lectin-domains that bind complex N-glycans clearly enhance affinity for target cells, contributing to the picomolar activity of this potent toxin. Disruption of this interaction may provide a potential therapy for bacterial infections that use a similar glycan-targeting mechanism.

Materials and Methods

Cloning of Truncated and Mutant VCC Proteins

Wild Type VCC (VCC_{WT}) and VCC truncated after Ala^{583} (VCC_{Trunc}) were cloned as described previously.[19] The isolated β-prism domain ($VCC_{\beta\text{-prism}}$) spanning residues Ser^{586}-Asn^{716} was amplified from VCC_{WT} by PCR and cloned between the NdeI and BamHI sites in the pET28b vector (Novagen) adding an amino-terminal 6x poly-histidine tag connected by a trypsin/thrombin site. Site-directed mutants were made by PCR[63] and confirmed by DNA sequencing.

Protein Expression

Full-length VCC proteinsand isolated lectin constructs were expressed in T7 Shuffle *E. coli* cells (New England Biolabs Inc.) and T7 Express *E. coli* cells, respectively. For every liter of expression culture, a 20 mL culture of overnight starter in the appropriate antibiotic was incubated overnight at 37 °C. Luria Broth was inoculated and incubated with constant shaking at 37 °C to an OD_{600} of 0.50–0.60. For VCC_{WT}, VCC_{Trunc}, and full-length mutants, cells were induced with 1 mM IPTG, and the culture grown for 4 hours with shaking at 30 °C. $VCC_{\beta\text{-prism}}$ constructs were grown for 8 hours at 37 °C and cells pelleted by centrifugation at 3500 × g for 20 minutes in a Sorvall ST 40R centrifuge. Cells were resuspended in 25 mL of buffer containing 20 mM TRIS pH 7.5, 150 mM NaCl, 0.25 mL protease inhibitor cocktail (Sigma), 1 mg DNAse, 1 mg lysozyme, 2.5 mM $CaCl_2$, 0.5 mM $MgCl_2$, and 10 mM imidazole and passed three times through a French press. Following centrifugation for 25 minutes at 15,000 rpm at 4 °C in a Sorvall SS-34 rotor, the supernatant was loaded on a pre-equilibrated 5 ml Ni-NTA column (GE Healthcare) and washed with 20 mM Tris pH 7.6, 150 mM NaCl buffer containing 40 mM imidazole. Proteins were eluted using a single step gradient of 250 mM imidazole and further purified over a Superdex 200 10/300 or 16/60 size exclusion column (GE Healthcare). Protein concentrations were determined spectrophotometrically by OD_{280} utilizing the calculated extinction coefficient for each construct. Circular dichroism spectra using a Jasco J-810 spectropolarimeter were used to confirm that mutants did not grossly disrupt the overall VCC secondary structure. We did not observe any decrease in β-sheet or increase in random coil characteristics.

Hemolytic Assays

Purified VCC was activated with a 1:350 ratio (weight:weight) of chymotrypsin in a buffer containing 20 mM Tris pH 7.5, 150 mM NaCl, and 10 mM $CaCl_2$. The reaction was stopped after a half hour by adding 20 mM EDTA and 1 mM PMSF. Activated protein was serially diluted into a lysis buffer containing 20 mM potassium phosphate pH 7.4, 150 mM NaCl, and 1 mg/ml BSA. Defibrinated rabbit whole blood (Becton Dickinson and Company) was added (190 μL per well) to a 96-well clear bottom plate to reach a final OD_{595} of 1.0 (approximately 1%). Activated protein dilutions (10 μL per well) were added and hemolysis monitored in real time by light scattering at 595 nm in a BioRad iMark microplate reader. Percent lysis at 30 minutes was calculated and standardized to VCC_{WT} (highest concentration with complete lysis) using the following expression: % lysis for $[n]$ = (OD_{595} at 0' - OD_{595} at 30')$_n$/ (OD_{595} at 0')$_n$ × 100. Standard deviations were calculated from data points collected in triplicate. For competition assays, serial dilutions of ligand were pre-incubated with the toxin for 5 minutes at room temperature before adding to blood. A baseline concentration of toxin was chosen that gave 75% total hemolysis after 30 minutes. Sigmoidal fits of the raw hemolysis data in triplicate were used to calculate the $t_{1/2}$ of lysis for each ligand concentration.

Isothermal Titration Calorimetry

For VCC_{WT}, the purified protein was concentrated to 100 μM and dialyzed against a buffer containing 5 mM TRIS pH 7.5. ITC was performed using a Microcal VP-ITC Isothermal Titration Calorimeter (MicroCal, LLC). To the sample cell, degassed protein (1.44 mL) was added and titrated with thirty 5 μL injections of 100 mM of Me-α-D-mannose with constant stirring at 25 °C. For $VCC_{\beta\text{-prism}}$, the protein was concentrated to 250 μM and titrated at 25 °C with injections of 150 mM Me-α-D-mannose and 75 mM of each of the following sugars: Me-α-D-glucose, Me-α-D-galactose, D-mannose, D-glucose, D-galactose, L-fucose, N-acetyl-D-glucosamine, Me-β-D-glucose, Me-β-D-galactose, cellobiose (glucose-β1,4-glucose), and maltose (glucose-α1,4-glucose). As a control, buffer alone was titrated with each sugar to calculate heat of dilution. Data were fit using a single-site model incorporated into Origin v. 7.0.

X-ray Crystallography

Purified $VCC_{\beta\text{-prism}}$ protein was run over a Superdex 200 16/60 size-exclusion column (GE Healthcare) in TBS buffer (20 mM Tris pH 7.5, 150 mM NaCl) and concentrated to 12 mg/ml. Crystals were obtained using the hanging-drop method in a condition containing 0.1 M ammonium acetate, 0.1 M Bis-tris pH 5.5, 25% PEG 3350, and 30 mM Me-α-mannose.

Crystals were briefly soaked in crystallization buffer containing 20% glycerol as a cryoprotectant and flash-cooled in liquid nitrogen. X-ray data were collected at a 1.54 Å wavelength using an Oxford Xcalibur Nova X-ray Generator with an Onyx CCD detector at 100 K. Data complete to 2.85 Å resolution were integrated, scaled and merged using CryAlisPro (Oxford Diffraction) and Scala.[64] The $VCC_{\beta\text{-prism}}$ crystals belonged to a $P3_12$ space group with unit cell dimensions of $a = 99.8$ Å, $b = 99.8$ Å, $c = 172.4$ Å, with $\alpha = \beta = 90°$ and $\gamma = 120°$. Molecular replacement using the isolated β-prism domain of VCC (PDB ID = 1XEZ) as a search model and Phaser[65] located six monomers in the asymmetric unit. Refinement was carried out using phenix_refine[66] with torsional NCS restraints. Five percent of the data were withheld from refinement to calculate R_{free} and iterative rebuilding was performed using Coot.[67]

Glycan Chip Assay

Purified VCC_{WT} and VCC_{Trunc} were labeled using primary amine chemistry with Alexa Fluor 488 dye using the Molecular Probes Alexa Fluor 488 Labeling Kit (Invitrogen) following the manufacturer's instructions. After removal of unbound dye on a 10 ml Mini Bio-Gel P-6 desalting column, labeling was confirmed by running the protein on a SDS-PAGE gel and imaged using a Typhoon FLA 9400 (GE Healthcare) imager. The labeling efficiency was calculated by absorbance at 494 nm (dye extinction coefficient = 71,000 $M^{-1}cm^{-1}$) to be 2.9 and 2.5 moles dye per mole of VCC_{WT} and VCC_{Trunc}, respectively.

Labeled VCC_{WT} and VCC_{Trunc} proteins were sent to the Consortium for Functional Glycomics (www.functionalglycomics.org) for analysis against the mammalian glycan screen version 5.0, which contains 611 glycans printed on Schott Nexterion H slides at a concentration of 100 μM. Chips were incubated for 1 hour in a dark humidified chamber with labeled protein at 1, 10, and 180 μg/mL concentrations, washed three times, dried under nitrogen, and imaged with a Perkin Elmer Microscanarray XL4000 scanner.[68] Image analysis was performed using Imagene (V.6) image analysis software. Each slide contains six copies of the glycan array, and the average response units and standard deviation are reported after dropping the highest and lowest point. The full results obtained from the screen are available publicly through the CFG website.

Fluorescence Anisotropy Binding Assay

The complex N-glycan, NGA2 (GlcNAcβ1-2Manα1-6(GlcNAcβ1-2Manα1-3)Manβ1-4GlcNAcβ1-4GlcNAc) was obtained from ProZyme Inc. with a 2-aminobenzoic acid fluorescent label attached to the core end. Fluorescence anisotropy binding assays were performed in triplicate in 20 mM Tris-HCl pH 7.5, 150 mM sodium chloride, and 1 mM EDTA. The β-prism domain was titrated into 100 nM 2-AA-NGA2 in a constant volume of 200 μL. To maintain a constant volume, an equal amount of titrand solution was removed from the cuvette prior to addition of titrant. Anisotropy measurements were made using a Jobin Yvon Fluoromax-4Spectrophotometer and 3 mm × 3 mm Starna Quartz Cuvettes. Samples were incubated at 15 °C for five minutes prior to excitation at 320 nm through 3.5 mm slits. Emission was measured at 410 nm and 520 nm through 15 mm slits. Four intensities were measured at each emission wavelength: I_{VV}, I_{VH}, I_{HV}, and I_{HH}, where the subscript denotes whether excitation and emission polarizers are mounted vertically or horizontally. Intensity

measurements were made six times at each wavelength with a one minute delay between each measurement. The six intensity measurements for each point were averaged. A corrected I_{VV} was calculated using the formula:

$$I_{VV} = I_{VV\ 410nm} - I_{VV\ Buffer\ 410nm} - (I_{VV\ 520nm} - I_{VV\ Buffer\ 520nm})$$

where $I_{VV\ 410nm}$ is the intensity of the sample at 410 nm with the excitation and emission polarizers mounted vertically; $I_{VV\ Buffer\ 410nm}$ is the intensity of the buffer at 410 nm with the excitation and emission polarizers mounted vertically; $I_{VV\ 520nm}$ is the intensity of the sample at 520 nm with the excitation and emission polarizers mounted vertically; and $I_{VV\ Buffer\ 520nm}$ is the intensity of the sample at 520 nm with the excitation and emission polarizers mounted vertically. A corrected I_{VH} was calculated using a similar equation, except the intensities were measured with a vertical excitation polarizer and a horizontal emission polarizer. Corrected intensity values were used to calculate the anisotropy using the formula:

$$\text{Anisotropy} = (I_{VV} - G \cdot I_{VH}) / (I_{VV} + 2(G \cdot I_{VH})$$

where G was experimentally determined to be 1.5. Anisotropy values were used to create a binding curve in Origin v. 6.0 and fit using the incorporated RandoA fitting equation.

Surface Plasmon Resonance

$VCC_{\beta\text{-prism}}$ protein was dialyzed into a buffer containing 10 mM HEPES pH 7.4 and 150 mM NaCl. Approximately 800 resonance units (RUs) of $VCC_{\beta\text{-prism}}$ were coupled to an activated carboxymethyl-dextran CM5 Biacore chip in a Biacore T100 SPR optical biosensor (GE Healthcare, Piscataway, NJ). Unlabeled NGA2 (ProZyme) was injected over the immobilized chip and a control chip without protein at a flow rate of 30 μl/min at concentrations of 0, 25, 50, 100, 200 (twice), 400, 600, 800, and 1000 nM in buffer containing 10 mM HEPES (pH 7.5), 150 mM NaCl, and 0.05% (vol/vol) surfactant P20. Experiments were performed at 25 °C. The titration data were analyzed by nonlinear curve fitting to a steady-state model using Biacore T100 analysis software (GE Healthcare, Piscataway, NJ).

Supplementary Material

Refer to Web version on PubMed Central for supplementary material.

Acknowledgments

We would like to thank Dr. Ishita Mukerji at Wesleyan for her help with fluorescence assays, George Korza from the University of Connecticut Health Center for assistance in collecting SPR data, and Esther Kim and Ryan Coffey for helping to characterize early VCC mutants. We would like to acknowledge the Consortium for Functional Glycomics funded by NIHGMS – GM62116 for obtaining glycan-array data. This work was supported by start-up funds from Wesleyan University and the Department of Molecular Biology. Research reported in this publication was supported by the National Institute of Allergy and Infectious Diseases of the National Institutes of Health under award number R15AI101977. The content is solely the responsibility of the authors and does not necessarily represent the official views of the National Institutes of Health.

Abbreviations

VCC	*Vibrio cholerae* cytolysin
β-PFT	β-pore-forming toxin
β-OG	β-octyl glucoside
ITC	isothermal titration calorimetry

NGA2	asialo-, agalacto-biantennary oligosaccharide
RUs	resonance units
rRBCs	rabbit red blood cells
RFUs	relative fluorescence units

References

1. World Health Organization. Weekly epidemiological record. 2011.
2. Zhu J, Miller MB, Vance RE, Dziejman M, Bassler BL, Mekalanos JJ. Quorum-sensing regulators control virulence gene expression in Vibrio cholerae. Proc. Natl. Acad. Sci. USA. 2002; 99:3129–3134. [PubMed: 11854465]
3. Olivier V, Haines GK 3rd, Tan Y, Satchell KJ. Hemolysin and the multifunctional autoprocessing RTX toxin are virulence factors during intestinal infection of mice with Vibrio cholerae El Tor O1 strains. Infect. Immun. 2007; 75:5035–5042. [PubMed: 17698573]
4. Olivier V, Queen J, Satchell KJ. Successful small intestine colonization of adult mice by Vibrio cholerae requires ketamine anesthesia and accessory toxins. PLoS One. 2009; 4:e7352. [PubMed: 19812690]
5. Zitzer A, Walev I, Palmer M, Bhakdi S. Characterization of Vibrio cholerae El Tor cytolysin as an oligomerizing pore-forming toxin. Med. Microbiol. Immunol. (Berl). 1995; 184:37–44. [PubMed: 8538577]
6. Zitzer A, Wassenaar TM, Walev I, Bhakdi S. Potent membrane-permeabilizing and cytocidal action of Vibrio cholerae cytolysin on human intestinal cells. Infect. Immun. 1997; 65:1293–1298. [PubMed: 9119464]
7. Valeva A, Walev I, Weis S, Boukhallouk F, Wassenaar TM, Bhakdi S. Pro-inflammatory feedback activation cycle evoked by attack of Vibrio cholerae cytolysin on human neutrophil granulocytes. Med. Microbiol. Immunol. 2008; 197:285–293. [PubMed: 17882454]
8. Larocque RC, Harris JB, Dziejman M, Li X, Khan AI, Faruque AS, Faruque SM, Nair GB, Ryan ET, Qadri F, Mekalanos JJ, Calderwood SB. Transcriptional profiling of Vibrio cholerae recovered directly from patient specimens during early and late stages of human infection. Infect.Immun. 2005; 73:4488–4493. [PubMed: 16040959]
9. Tsou AM, Zhu J. Quorum sensing negatively regulates hemolysin transcriptionally and posttranslationally in Vibrio cholerae. Infect.Immun. 2010; 78:461–467. [PubMed: 19858311]
10. Queen J, Satchell KJ. Neutrophils are essential for containment of Vibrio cholerae to the intestine during the proinflammatory phase of infection. Infect.Immun. 2012; 80:2905–2913. [PubMed: 22615254]
11. Song L, Hobaugh MR, Shustak C, Cheley S, Bayley H, Gouaux JE. Structure of staphylococcal α-hemolysin, a heptameric transmembrane pore. Science. 1996; 274:1859–1866. [PubMed: 8943190]
12. Yamashita K, Kawai Y, Tanaka Y, Hirano N, Kaneko J, Tomita N, Ohta M, Kamio Y, Yao M, Tanaka I. Crystal structure of the octameric pore of staphylococcal γ-hemolysin reveals the β-barrel pore formation mechanism by two components. Proc. Natl. Acad. of Sci.USA. 2011; 108:17314–17319. [PubMed: 21969538]
13. De S, Olson R. Crystal structure of the Vibrio cholerae cytolysin heptamer reveals common features among disparate pore-forming toxins. Proc. Natl. Acad. of Sci.USA. 2011; 108:7385–7390. [PubMed: 21502531]
14. Abrami L, van Der Goot FG. Plasma membrane microdomains act as concentration platforms to facilitate intoxication by aerolysin. J. Cell Biol. 1999; 147:175–184. [PubMed: 10508864]
15. Walker B, Braha O, Cheley S, Bayley H. An intermediate in the assembly of a pore-forming protein trapped with a genetically-engineered switch. Chem. Biol. 1995; 2:99–105. [PubMed: 9383410]

16. Eidels L, Proia RL, Hart DA. Membrane receptors for bacterial toxins. Microbiol.Rev. 1983; 47:596–620. [PubMed: 6363900]

17. Iacovache I, van der Goot FG, Pernot L. Pore formation: an ancient yet complex form of attack. Biochim. Biophys. Acta. 2008; 1778:1611–1623. [PubMed: 18298943]

18. Farrand S, Hotze E, Friese P, Hollingshead SK, Smith DF, Cummings RD, Dale GL, Tweten RK. Characterization of a streptococcal cholesterol-dependent cytolysin with a lewis y and b specific lectin domain. Biochemistry. 2008; 47:7097–7107. [PubMed: 18553932]

19. Olson R, Gouaux E. Crystal structure of the Vibrio cholerae cytolysin (VCC) pro-toxin and its assembly into a heptameric transmembrane pore. J. Mol. Biol. 2005; 350:997–1016. [PubMed: 15978620]

20. Rutenber E, Ready M, Robertus JD. Structure and evolution of ricin B chain. Nature. 1987; 326:624–626. [PubMed: 3561502]

21. Liu Y, Chirino AJ, Misulovin Z, Leteux C, Feizi T, Nussenzweig MC, Bjorkman PJ. Crystal structure of the cysteine-rich domain of mannose receptor complexed with a sulfated carbohydrate ligand. J. Exp. Med. 2000; 191:1105–1116. [PubMed: 10748229]

22. Jeyaprakash AA, Srivastav A, Surolia A, Vijayan M. Structural basis for the carbohydrate specificities of artocarpin: variation in the length of a loop as a strategy for generating ligand specificity. J. Mol. Biol. 2004; 338:757–770. [PubMed: 15099743]

23. Sankaranarayanan R, Sekar K, Banerjee R, Sharma V, Surolia A, Vijayan M. A novel mode of carbohydrate recognition in jacalin, a Moraceae plant lectin with a β-prism fold. Nat. Struct. Biol. 1996; 3:596–603. [PubMed: 8673603]

24. Ziolkowska NE, O'Keefe BR, Mori T, Zhu C, Giomarelli B, Vojdani F, Palmer KE, McMahon JB, Wlodawer A. Domain-swapped structure of the potent antiviral protein griffithsin and its mode of carbohydrate binding. Structure. 2006; 14:1127–1135. [PubMed: 16843894]

25. Lee X, Thompson A, Zhang Z, Ton-that H, Biesterfeldt J, Ogata C, Xu L, Johnston RA, Young NM. Structure of the complex of Maclura pomifera agglutinin and the T-antigen disaccharide, Galβ1,3GalNAc. J. Biol. Chem. 1998; 273:6312–6318. [PubMed: 9497359]

26. Li JD, Carroll J, Ellar DJ. Crystal structure of insecticidal Δ-endotoxin from Bacillus thuringiensis at 2.5 Å resolution. Nature. 1991; 353:815–821. [PubMed: 1658659]

27. Saha N, Banerjee KK. Carbohydrate-mediated regulation of interaction of Vibrio cholerae hemolysin with erythrocyte and phospholipid vesicle. J. Biol. Chem. 1997; 272:162–167. [PubMed: 8995242]

28. Dutta S, Mazumdar B, Banerjee KK, Ghosh AN. Three-dimensional structure of different functional forms of the Vibrio cholerae hemolysin oligomer: a cryo-electron microscopic study. J.Bacteriol. 2010; 192:169–178. [PubMed: 19854900]

29. He Y, Olson R. Three-dimensional structure of the detergent-solubilized Vibrio cholerae cytolysin (VCC) heptamer by electron cryomicroscopy. J. Struct. Biol. 2010; 169:6–13. [PubMed: 19616104]

30. Dutta S, Mazumdar B, Banerjee KK, Ghosh AN. Three-dimensional structure of different functional forms of the Vibrio cholerae hemolysin oligomer: a cryo-electron microscopic study. J. Bacteriol. 192:169–178. [PubMed: 19854900]

31. Pettersen EF, Goddard TD, Huang CC, Couch GS, Greenblatt DM, Meng EC, Ferrin TE. UCSF Chimera--a visualization system for exploratory research and analysis. J. Comput. Chem. 2004; 25:1605–1612. [PubMed: 15264254]

32. Mills JE, Dean PM. Three-dimensional hydrogen-bond geometry and probability information from a crystal survey. J.Comput. Aided Mol. Des. 1996; 10:607–622. [PubMed: 9007693]

33. Drickamer K, Taylor ME. Glycan arrays for functional glycomics. Genome Biol. 2002; 3:REVIEWS1034. [PubMed: 12537579]

34. Varki, A.; Cummings, RD.; Esko, JD.; Freeze, HH.; Stanley, P.; Bertozzi, CR.; Hart, GW.; Etzler, ME. Essentials of Glycobiology. 2nd ed. Cold Spring Harbor, New York: Cold Spring Harbor Laboratory Press; 2009. edit

35. Ikigai H, Akatsuka A, Tsujiyama H, Nakae T, Shimamura T. Mechanism of membrane damage by El Tor hemolysin of Vibrio cholerae O1. Infect. Immun. 1996; 64:2968–2973. [PubMed: 8757822]

36. Miyata ST, Kitaoka M, Wieteska L, Frech C, Chen N, Pukatzki S. The Vibrio Cholerae Type VI Secretion System: Evaluating its Role in the Human Disease Cholera. Front.Microbiol. 2010; 1:117. [PubMed: 21607085]
37. Pukatzki S, Ma AT, Sturtevant D, Krastins B, Sarracino D, Nelson WC, Heidelberg JF, Mekalanos JJ. Identification of a conserved bacterial protein secretion system in Vibrio cholerae using the Dictyostelium host model system. Proc. Natl. Acad. Sci. USA. 2006; 103:1528–1533. [PubMed: 16432199]
38. Beneteau J, Renard D, Marche L, Douville E, Lavenant L, Rahbe Y, Dupont D, Vilaine F, Dinant S. Binding properties of the N-acetylglucosamine and high-mannose N-glycan PP2-A1 phloem lectin in Arabidopsis. Plant Physiol. 2010; 153:1345–1361. [PubMed: 20442276]
39. Hung LD, Sato Y, Hori K. High-mannose N-glycan-specific lectin from the red alga Kappaphycus striatum (Carrageenophyte). Phytochem. 2011; 72:855–861.
40. Al Atalah B, Fouquaert E, Vanderschaeghe D, Proost P, Balzarini J, Smith DF, Rouge P, Lasanajak Y, Callewaert N, Van Damme EJ. Expression analysis of the nucleocytoplasmic lectin 'Orysata' from rice in Pichia pastoris. FEBS J. 2011; 278:2064–2079. [PubMed: 21481190]
41. Nagre NN, Chachai VB, Sundaram PM, Naik RS, Pujari R, Shastry P, Swamy BM, Inamdar SR. A potent mitogenic lectin from the mycelia of a phytopathogenic fungus, Rhizoctonia bataticola, with complex sugar specificity and cytotoxic effect on human ovarian cancer cells. Glycoconj.J. 2010; 27:375–386. [PubMed: 20306342]
42. Fouquaert E, Smith DF, Peumans WJ, Proost P, Balzarini J, Savvides SN, Damme EJ. Related lectins from snowdrop and maize differ in their carbohydrate-binding specificity. Biochem.Biophys.Res.Commun. 2009; 380:260–265. [PubMed: 19167365]
43. Gourdine JP, Cioci G, Miguet L, Unverzagt C, Silva DV, Varrot A, Gautier C, Smith-Ravin EJ, Imberty A. High affinity interaction between a bivalve C-type lectin and a biantennary complex-type N-glycan revealed by crystallography and microcalorimetry. J.Biol.Chem. 2008; 283:30112–30120. [PubMed: 18687680]
44. Kerr MA, Stocks SC. The role of CD15-(Le(X))-related carbohydrates in neutrophil adhesion. Histochem J. 1992; 24:811–826. [PubMed: 1362195]
45. Torii A, Nakayama A, Harada A, Nakao A, Nonami T, Sakamoto J, Watanabe T, Ito M, Takagi H. Expression of the CD15 antigen in hepatocellular carcinoma. Cancer. 1993; 71:3864–3867. [PubMed: 7685236]
46. Malagolini N, Santini D, Chiricolo M, Dall'Olio F. Biosynthesis and expression of the Sda and sialyl Lewis×antigens in normal and cancer colon. Glycobiology. 2007; 17:688–697. [PubMed: 17395692]
47. Mahdavi J, Sonden B, Hurtig M, Olfat FO, Forsberg L, Roche N, Angstrom J, Larsson T, Teneberg S, Karlsson KA, Altraja S, Wadstrom T, Kersulyte D, Berg DE, Dubois A, Petersson C, Magnusson KE, Norberg T, Lindh F, Lundskog BB, Arnqvist A, Hammarstrom L, Boren T. Helicobacter pylori SabA adhesin in persistent infection and chronic inflammation. Science. 2002; 297:573–578. [PubMed: 12142529]
48. Tucker KD, Wilkins TD. Toxin A of Clostridium difficile binds to the human carbohydrate antigens I, X, and Y. Infect. Immun. 1991; 59:73–78. [PubMed: 1670930]
49. Chung MC, Wines BD, Baker H, Langley RJ, Baker EN, Fraser JD. The crystal structure of staphylococcal superantigen-like protein 11 in complex with sialyl Lewis X reveals the mechanism for cell binding and immune inhibition. Mol.Microbiol. 2007; 66:1342–1355. [PubMed: 18045383]
50. Nakayama F, Nishihara S, Iwasaki H, Kudo T, Okubo R, Kaneko M, Nakamura M, Karube M, Sasaki K, Narimatsu H. CD15 expression in mature granulocytes is determined by α1,3-fucosyltransferase IX, but in promyelocytes and monocytes by α1,3-fucosyltransferase IV. J. Biol. Chem. 2001; 276:16100–16106. [PubMed: 11278338]
51. Croce MV, Isla-Larrain M, Rabassa ME, Demichelis S, Colussi AG, Crespo M, Lacunza E, Segal-Eiras A. Lewis×is highly expressed in normal tissues: a comparative immunohistochemical study and literature revision. Pathol.Oncol.Res. 2007; 13:130–138. [PubMed: 17607374]
52. Olivier V, Salzman NH, Satchell KJ. Prolonged colonization of mice by Vibrio cholerae El Tor O1 depends on accessory toxins. Infect. Immun. 2007; 75:5043–5051. [PubMed: 17698571]

53. Yu LG. The oncofetal Thomsen-Friedenreich carbohydrate antigen in cancer progression. Glycoconj.J. 2007; 24:411–420. [PubMed: 17457671]
54. van den Akker F, Steensma E, Hol WG. Tumor marker disaccharide D-Gal-β1,3-GalNAc complexed to heat-labile enterotoxin from Escherichia coli. Protein Sci. 1996; 5:1184–1188. [PubMed: 8762150]
55. Baenziger JU, Fiete D. Structure of the complex oligosaccharides of fetuin. J. Biol. Chem. 1979; 254:789–795. [PubMed: 83994]
56. Green ED, Adelt G, Baenziger JU, Wilson S, Van Halbeek H. The asparagine-linked oligosaccharides on bovine fetuin. Structural analysis of N-glycanase-released oligosaccharides by 500-megahertz 1H NMR spectroscopy. J. Biol. Chem. 1988; 263:18253–18268. [PubMed: 2461366]
57. Yet MG, Chin CC, Wold F. The covalent structure of individual N-linked glycopeptides from ovomucoid and asialofetuin. J. Biol. Chem. 1988; 263:111–117. [PubMed: 2447075]
58. Connaris H, Crocker PR, Taylor GL. Enhancing the receptor affinity of the sialic acid-binding domain of Vibrio cholerae sialidase through multivalency. J. Biol. Chem. 2009; 284:7339–7351. [PubMed: 19124471]
59. Nagamune K, Yamamoto K, Honda T. Cloning and sequencing of a novel hemolysis gene of Vibrio cholerae. FEMS Microbiol Lett. 1995; 128:265–269. [PubMed: 7781973]
60. Clark GF, Oehninger S, Seppala M. Role for glycoconjugates in cellular communication in the human reproductive system. Mol.Hum.Reprod. 1996; 2:513–517. [PubMed: 9239661]
61. Sutton-Smith M, Wong NK, Khoo KH, Wu SW, Yu SY, Patankar MS, Easton R, Lattanzio FA, Morris HR, Dell A, Clark GF. Analysis of protein-linked glycosylation in a sperm-somatic cell adhesion system. Glycobiology. 2007; 17:553–567. [PubMed: 17337520]
62. Wilke GA, Bubeck Wardenburg J. Role of a disintegrin and metalloprotease 10 in Staphylococcus aureus α-hemolysin-mediated cellular injury. Proc. Natl. Acad. Sci. USA. 2010; 107:13473–13478. [PubMed: 20624979]
63. Fisher CL, Pei GK. Modification of a PCR-based site-directed mutagenesis method. BioTechniques. 1997; 23:570–571. 574. [PubMed: 9343663]
64. CCP4 P. The CCP4 suite: programs for protein crystallography. Acta Crystallogr. D Biol. Crystallogr. 1994; 50:760–763. [PubMed: 15299374]
65. McCoy AJ, Grosse-Kunstleve RW, Adams PD, Winn MD, Storoni LC, Read RJ. Phaser crystallographic software. J.Appl.Crystallogr. 2007; 40:658–674. [PubMed: 19461840]
66. Afonine PV, Grosse-Kunstleve RW, Echols N, Headd JJ, Moriarty NW, Mustyakimov M, Terwilliger TC, Urzhumtsev A, Zwart PH, Adams PD. Towards automated crystallographic structure refinement with phenix.refine. Acta Crystallogr. D Biol. Crystallogr. 2012; 68:352–367. [PubMed: 22505256]
67. Emsley P, Cowtan K. Coot: model-building tools for molecular graphics. Acta Crystallogr. D Biol. Crystallogr. 2004; 60:2126–2132. [PubMed: 15572765]
68. Blixt O, Head S, Mondala T, Scanlan C, Huflejt ME, Alvarez R, Bryan MC, Fazio F, Calarese D, Stevens J, Razi N, Stevens DJ, Skehel JJ, van Die I, Burton DR, Wilson IA, Cummings R, Bovin N, Wong CH, Paulson JC. Printed covalent glycan array for ligand profiling of diverse glycan binding proteins. Proc. Natl. Acad. Sci. USA. 2004; 101:17033–17038. [PubMed: 15563589]

Highlights

- Vibrio cholerae cytolysin (VCC) is a pore-forming toxin with lectin-like domains
- The β-prism domain binds glucoside and mannoside monosaccharides weakly
- The β-prism domain preferentially binds the heptasaccharide core of N-glycans
- The affinity for the N-glycan core was measured at roughly 100 nM
- We have identified specific cell-surface carbohydrate motifs targeted by VCC

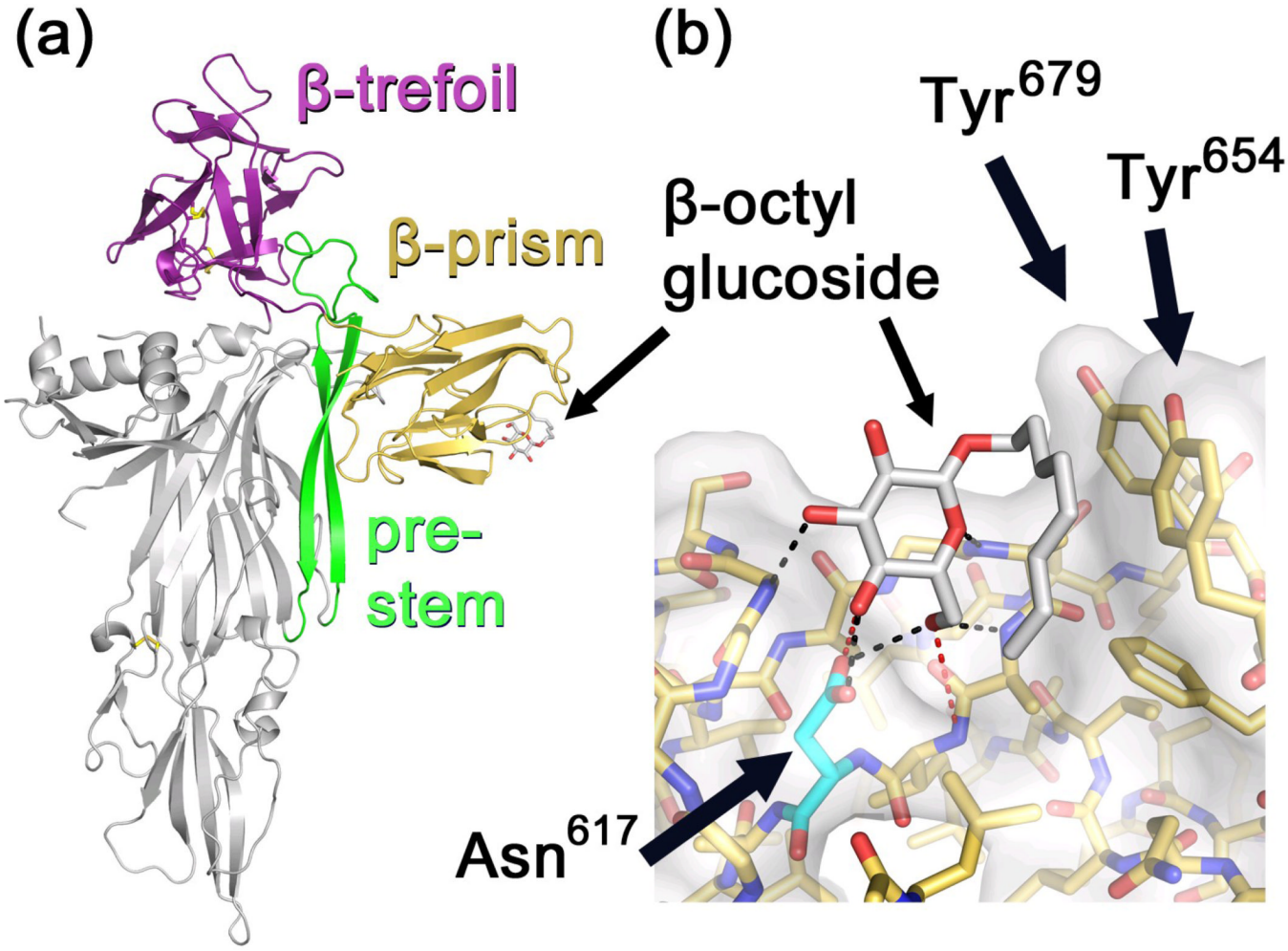

Figure 1.

Structure of VCC illustrating putative carbohydrate-binding domains. (a) Crystal structure of VCC (PDB 1XEZ) with β-trefoil domain colored magenta and β-prism domain colored gold. A molecule of β–octyl glucoside is shown bound within a shallow pocket in the β-prism domain. The amphipathic pre-stem loop that forms the membrane-spanning channel in the assembled heptamer is colored green. (b) Close-up view of the carbohydrate binding pocket. Hydrogen bonds between the ligand and protein were identified using the FindHBond function implemented in Chimera[31,32] with strict geometric criteria indicated in black and relaxed criteria in red. All putative hydrogen bonds are between ligand and backbone atoms except for bonds between O4, O6, and Asn^{617}.

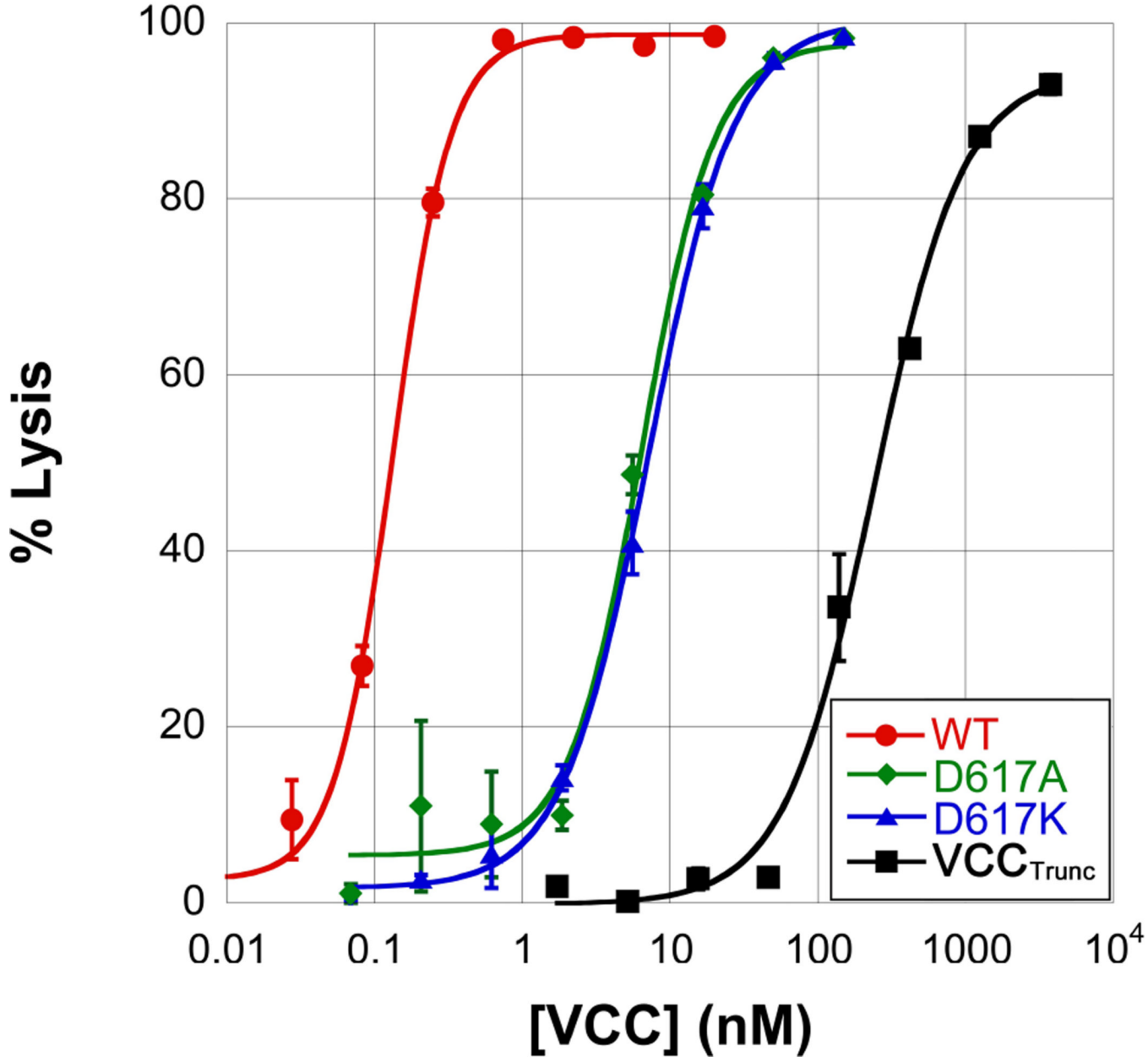

Figure 2.

Hemolysis assays of VCC mutants. Purified VCC was added to a sample of 1% rabbit whole blood and monitored for lysis by the change in absorbance at 590 nm. Wild-type VCC lyses 50% of the blood sample in 30 minutes at a concentration of approximately 100 pM. Mutation of Asn^{617} to alanine or lysine results in a roughly 50-fold decrease in hemolytic activity as measured by this assay. Complete removal of the β-prism domain results in more than a 1000-fold decrease in hemolytic activity.

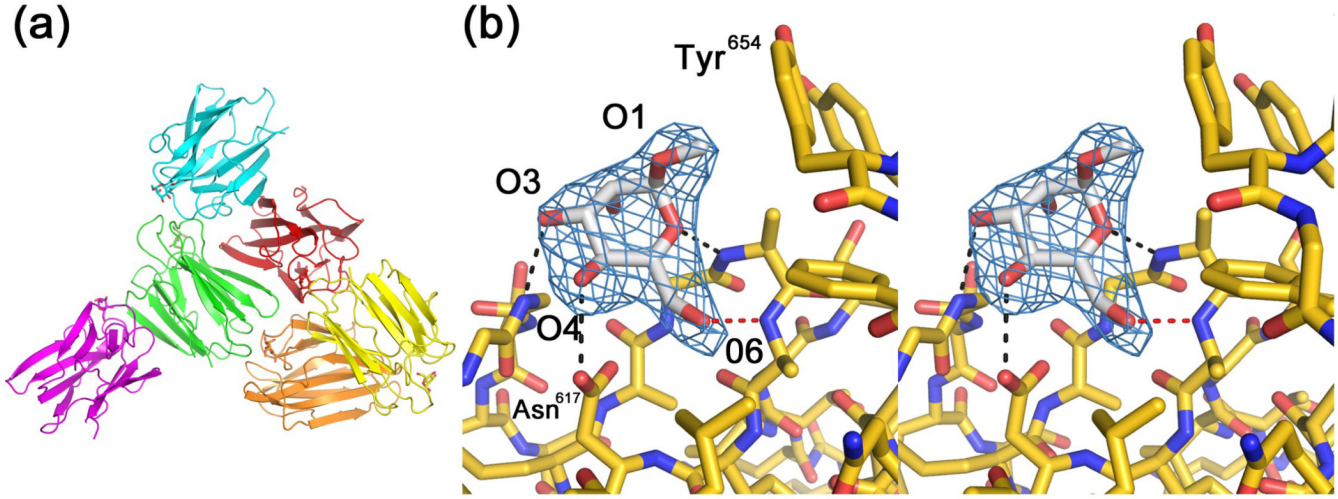

Figure 3.

Crystal structure of the isolated β-prism domain with Me-α-mannose bound. (a) The asymmetric unit of the crystal contains six copies of the β-prism domain, each containing a single bound Me-α-mannose molecule (shown in stick representation). (b) Stereo view showing a close up of the Me-α-mannose bound to VCC. Electron density from a F_o-F_c electron density map where the ligand was omitted from the model structure factor calculation is shown in blue mesh contoured at a level of 3.0 σ. Putative hydrogen bonds are represented as described in Figure 1.

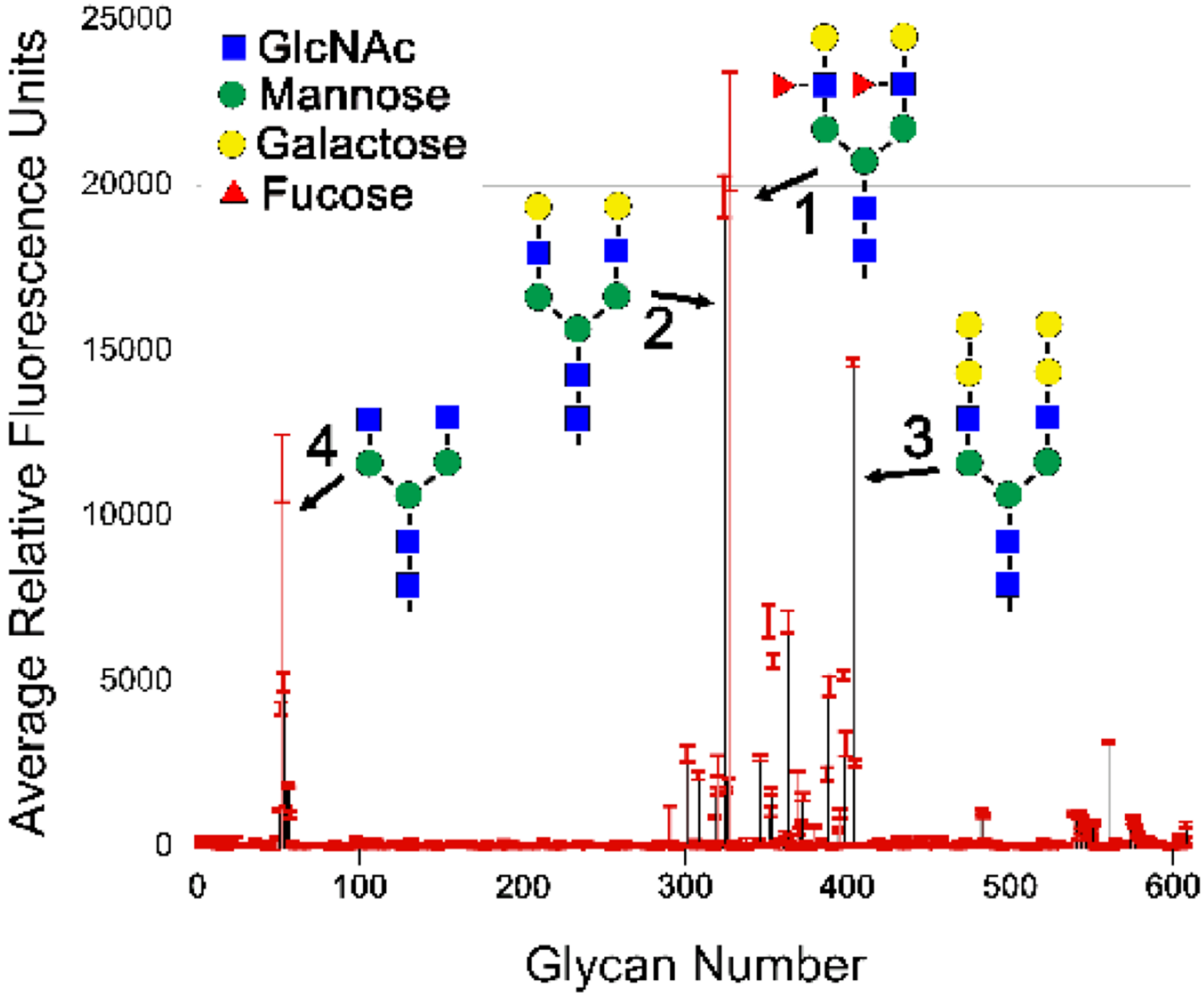

Figure 4.

VCC glycan screen results. Purified VCC was labeled with Alexa Fluor 488 and screened against an array of 611 mammalian glycans by the Consortium for Functional Glycomics. The average fluorescence of VCC binding to each glycan is shown with red error bars indicating the standard deviation from four replicates (after the highest and lowest replicates were dropped). The top four hits are illustrated in schematic form and all contain a bi-antennary N-glycan heptasaccharide core. A detailed list of the 25 top hits is shown in Supplementary Figure S5 and variants of the top hits that exhibited low binding is shown in Figure S6.

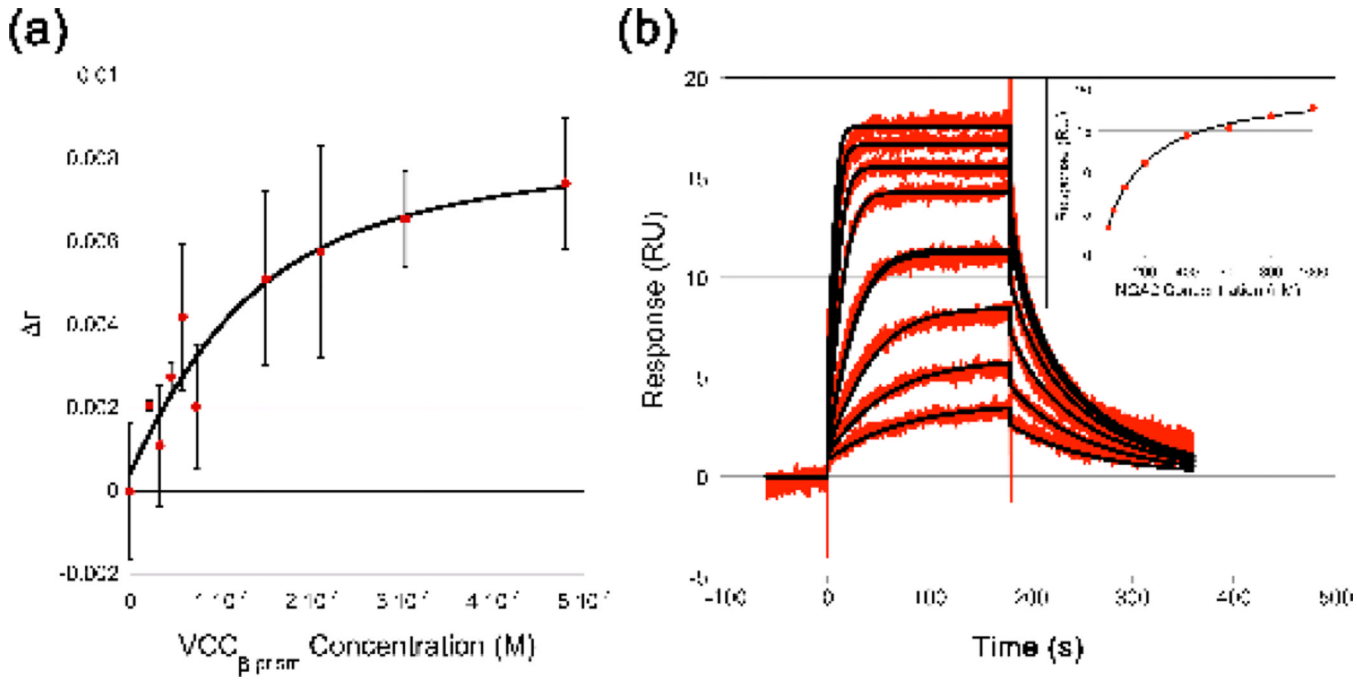

Figure 5.

Purified VCC β-prism domain binds the heptasaccharide NGA2 with nanomolar affinity. (a) Fluorescence anisotropy of a solution of 100 nM of 2AA-labled NGA2 was monitored as purified β-prism domain was titrated into the cuvette. A fit of the data from three replicates using the RandoA model in Origin 6.0 indicated a dissociation constant of 71.3 nM ± 65.4 nM. (b) Surface plasmon resonance was used to measure the affinity of VCC for NGA2. The VCC β-prism domain was coupled to a CM5 chip and probed with 25, 50, 100, 200 (twice), 400, 600, 800, and 1000 nM of NGA2 using a Biacore T100 spectrometer. Data were fit to kinetic and equilibrium (inset) single site models. The kinetic fit indicated a K_D of 108 nM with a k_a of 37,000 $M^{-1}s^{-1}$ and a k_d of 0.04 s^{-1}. The equilibrium analysis indicated K_D of 183 nM.

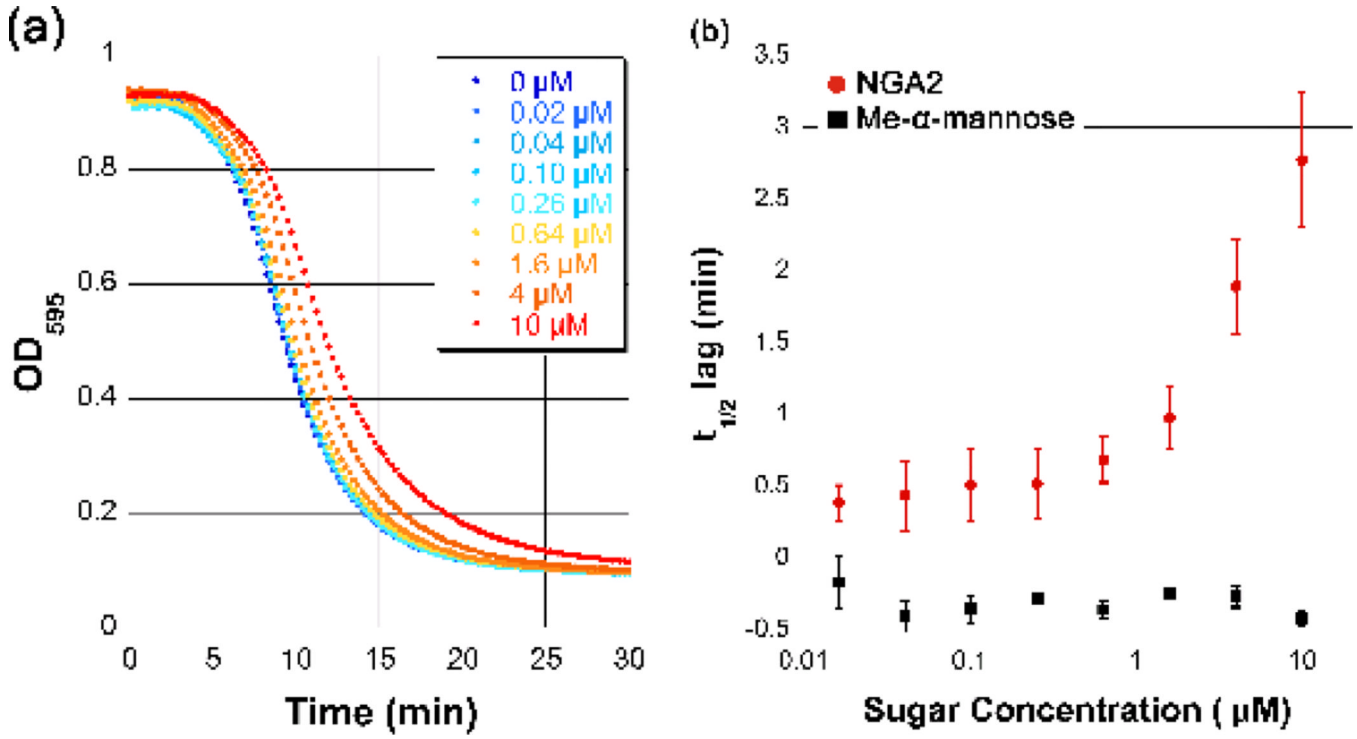

Figure 6.

Competition of VCC hemolytic activity by NGA2. (a) Preincubation of wild-type VCC with the NGA2 heptasaccharide core led to a concentration-dependent lag in the half-life of rabbit blood hemolysis. The change in absorbance at 590 nm over time is shown for increasing amounts of NGA2 up to 10 μM concentration. (b) Hemolytic data were fit using a sigmoidal function in KaleidaGraph v. 4.1.3 (Synergy Software) to extract the time required to reach 50% lysis. The lag in the $t_{1/2}$ in minutes was plotted for the average of three replicates for NGA2 and for Me-α-mannose within the same concentration range. The nanomolar affinity NGA2 showed a concentration-dependent lag whereas the millimolar affinity Me-α-mannose showed no effect.

Table 1

Isothermal titration calorimetry data for $VCC_{\beta\text{-prism}}$

Compound	N	K_D (mM)	ΔG (cal/mol)
Me-α-Mannose	0.967	3.24 ± 0.10	−3424
Me-α-Glucose	0.986	7.09 ± 0.15	−2944
Glucose	0.916	12.0 ± 0.60	−2679
Mannose	0.984	14.8 ± 1.18	−2456
Maltose (Glcα1-4Glc)	1.000	30.9 ± 3.17	−2090

Binding was not detected with Me-α-Galactose, Me-β-Glucose, Me-β-Galactose, Galactose, Fucose, N-acetylglucosamine, or cellobiose (Glcβ1-4Glc)